Chemical Geology 258 (2009) 125–135

Contents lists available at ScienceDirect

Chemical Geology

journal homepage: www.elsevier.com/locate/chemgeo

Coupled alkali-feldspar dissolution and secondary mineral precipitation in batch systems: 1. New experiments at 200 °C and 300 bars

Qi Fu [a,*], Peng Lu [b], Hiromi Konishi [b,1], Robert Dilmore [c], Huifang Xu [d], W.E. Seyfried Jr. [a], Chen Zhu [b]

[a] Department of Geology and Geophysics, University of Minnesota, Minneapolis, MN 55455, USA
[b] Department of Geological Sciences, Indiana University, Bloomington, IN 47405, USA
[c] National Energy Technology Laboratory, U. S. Department of Energy, Pittsburgh, PA 15236, USA
[d] Department of Geology and Geophysics, University of Wisconsin-Madison, Madison, WI 53706, USA

ARTICLE INFO

Article history:
Received 18 February 2008
Received in revised form 15 September 2008
Accepted 16 September 2008

Editor: J. Fein

Keywords:
Feldspar
Kinetics
Dissolution
Precipitation
Secondary minerals
Mass transfer

ABSTRACT

Batch reactor experiments were conducted to assess perthitic alkali-feldspar dissolution and secondary mineral formation in an initially acidic fluid (pH=3.1) at 200 °C and 300 bars. Temporal evolution of fluid chemistry was monitored by major element analysis of *in situ* fluid samples. Solid reaction products were retrieved from two identical experiments terminated after 5 and 78 days. Scanning electron microscopy revealed dissolution features and significant secondary mineral coverage on feldspar surfaces. Boehmite and kaolinite were identified as secondary minerals by X-ray diffraction and transmission electron microscopy. X-ray photoelectron spectroscopy analysis of alkali-feldspar surfaces before and after reaction showed a trend of increasing Al/Si ratios and decreasing K/Al ratios with reaction progress, consistent with the formation of boehmite and kaolinite.

Saturation indices of feldspars and secondary minerals suggest that albite dissolution occurred throughout the experiments, while K-feldspar exceeded saturation after 216 h of reaction. Reactions proceeded slowly and full equilibrium was not achieved, the relatively high temperature of the experiments notwithstanding. Thus, time series observations indicate continuous supersaturation with respect to boehmite and kaolinite, although the extent of this decreased with reaction progress as the driving force for albite dissolution decreased. The first experimental evidence of metastable co-existence of boehmite, kaolinite and alkali feldspar in the feldspar hydrolysis system is consistent with theoretical models of mineral dissolution/precipitation kinetics where the ratio of the secondary mineral precipitation rate constant to the rate constant of feldspar dissolution is well below unity. This has important implications for modeling the time-dependent evolution of feldspar dissolution and secondary mineral formation in natural systems.

1. Introduction

Silicate mineral dissolution and secondary mineral precipitation are integrated processes in chemical weathering and hydrothermal alteration of rocks. Numerous experiments have been conducted for measuring silicate mineral dissolution rates (Busenburg and Clemency, 1976; Holdren and Berner, 1979; Chou and Wollast, 1985; Knauss and Wolery, 1986; Nagy et al., 1991; Nagy and Lasaga, 1992; Burch et al., 1993; Gautier et al., 1994; Hellmann, 1994; Oelkers et al., 1994; Hellmann, 1995; Nagy, 1995; Stillings and Brantley, 1995; Brantley and Stillings, 1996). The primary focus of many of these studies, however, was to derive mineral dissolution rates from steady state chemical conditions. In such experiments, silicate minerals, mostly feldspars, are dissolved far from equilibrium and secondary mineral precipitation is avoided by adjusting the chemistry and rate of recirculation of the fluid phase. Results of these experiments have been enormously successful, providing a wealth of data on the rate and mechanism of mineral dissolution processes under a wide range of chemical and physical conditions.

Batch reactor experiments of feldspar hydrolysis, on the other hand, provide a different set of data, which address the broader context of congruency and incongruency, phase relations, mineral metastability, and interconnections between dissolution and precipitation reactions. Tremendous progress in our understanding of feldspar hydrolysis in closed systems has come from the seminal work by Helgeson and co-workers (Helgeson, 1968; Helgeson et al., 1969, 1970; Helgeson, 1971, 1972, 1974, 1979; Helgeson et al., 1984). While the first feldspar hydrolysis experiments conducted in batch

* Corresponding author. Tel.: +1 612 624 9593; fax: +1 612 625 3819.
E-mail address: fuxx0033@umn.edu (Q. Fu).
[1] Present address: Department of Geology and Geophysics, University of Wisconsin-Madison, Madison, WI 53706, USA.

0009-2541/$ – see front matter © 2008 Elsevier B.V. All rights reserved.
doi:10.1016/j.chemgeo.2008.09.014

reactors provided valuable information on the mechanism of feldspar dissolution, as summarized in Helgeson (1971) and Petrovic (1976), technological development of experimental design and apparatus has allowed the sampling of fluid co-existing with minerals at a wide range of temperatures and pressures (Seyfried et al., 1987). Furthermore, electron microscopy and surface analytical techniques have advanced significantly, which allow more accurate identification of secondary minerals, even when such phases exist on the nanometer size scale (Penn et al., 2001; Zhu et al., 2006).

Here we report results of alkali-feldspar dissolution experiments in well-mixed batch reactors that were performed at 200 °C and 300 bars in order to examine mineral dissolution and precipitation processes in moderately acidic fluids. Although dissolution reactions of single feldspars have been reported in the literature (Busenburg and Clemency, 1976; Holdren and Berner, 1979; Helgeson et al., 1984; Chou and Wollast, 1985; Knauss and Wolery, 1986; Wollast and Chou, 1992; Gautier et al., 1994; Hellmann, 1994; Oelkers et al., 1994; Hellmann, 1995; Stillings and Brantley, 1995; Brantley and Stillings, 1996; Hellmann and Tisserand, 2006), only a few experimental studies have been performed on feldspars with complex compositions (Morey and Fournier, 1961; Lagache, 1976; Rafal'skiy et al., 1990; Tsuchiya et al., 1995). The combination of time series monitoring of fluid chemistry and mineral analysis (scanning electron microscopy (SEM), high resolution transmission electron microscopy (HRTEM), X-ray diffraction (XRD), X-ray photoelectron spectroscopy (XPS), and electron microprobe analysis (EMPA)) at different reaction stages represents an insightful experimental strategy to assess geochemical controls on the temporal evolution of minerals and coexisting fluids. While this approach is relevant to mass transfer processes in a variety of natural and engineered hydrologic and hydrothermal rock–fluid systems, the experimental data are important in that they form a basis for evaluating a number of theories and hypotheses on the kinetics of water–rock interactions.

2. Experiments

Two batch experiments, with run times of 1872 h (78 days) and 120 h (5 days), involving perthitic alkali-feldspar dissolution in K-bearing (~0.20 KCl mol/kg) fluid at 200 °C, 300 bars were conducted at the University of Minnesota and National Energy Technology Laboratory (NETL), respectively. 40 g KCl solution and 1.5 g alkali-feldspar were used for both experiments. Prior to the experiments, the starting fluid was acidified to pH = 3.0 by addition of dilute HCl, so as to create initial conditions far from equilibrium.

"Orthoclase" crystals having an average size of ~0.5 cm were obtained from WARD'S Natural Sciences Establishment. The crystals were ground with an agate mortar and pestle, and subsequently dry sieved to retain the size fraction between 50 and 100 μm. For the freshly ground material, there were a large number of submicron-to-micron size particles that adhered to the surface of large grains. To remove these particles, the feldspar sample was first ultrasonically "cleaned" in analytical grade acetone, and then repeatedly rinsed with deionized water, prior to drying at 105 °C.

A Beckman Coulter SA-3100 was used for BET surface area analysis of alkali-feldspar samples before experiments. The instrument was calibrated before and after measurements, using NIST reference material 1900, a silicon nitrite powder with surface area of 2.85 m^2/g. Multipoint N_2 gas adsorption isotherms were measured to obtain the specific surface area of 0.13 m^2/g (±5%) for the alkali-feldspar reactant.

The alkali-feldspar and acidified KCl solution were loaded into a flexible Au/Ti reaction cell and placed in a steel-alloy autoclave following procedures described in Seyfried et al. (1987). The reaction cell allows sampling of aqueous fluid from the ongoing reaction at constant temperature and pressure. Thus, internally filtered fluid samples could be recovered from the reaction cell any time during an experiment.

Fluid samples were analyzed for major dissolved components. Anion analyses were conducted on a Dionex ICS-2000 ion chromatography (IC) system composed of an AS 19 column (4 mm ID) and an ASRS self-regenerating suppressor (4 mm ID). KOH solution was used as the eluent at flow rate of 1 ml/min. Gradient eluent concentrations were programmed as follows: 4 mM for 30 min, 10 mM for 30 min and 25 mM for 15 min. The column temperature and cell temperature were constant at 30 °C. The injection volume of each sample was 50.0 μl. Uncertainties in reported concentrations were estimated to be within ±1%.

Major cation analyses were conducted on a Thermo Elemental PQ ExCell quadrupole inductively coupled plasma mass spectrometer (ICP-MS) with a simultaneous analog and pulse counting detector. System calibration was accomplished by using NIST traceable single or multi-element standard solutions. For each sample, standards and blanks were repeated 5 times to determine the mean and standard deviation for each selected elemental mass. All standards, blanks, and samples were atomized and introduced into a standard Meinhardt nebulizer by a free aspiration rate of approximately 1 ml/min. All elements were measured on the most appropriate mass by peak hopping with dwell times of approximately 35 μs per mass and 25–50 mass sweeps per replicate. The clean matrix acid was used to flush the system for a minimum time of 65 s to prevent carryover between samples. Uncertainties for all elements were estimated to be within ±1%.

The pH of all fluid samples was measured at ambient laboratory conditions using a THERMO combination glass pH/reference electrode and Accumet AR-20 meter. Prior to measurement, the pH electrode was calibrated with NIST pH standard buffers, 4.0 and 7.0. Replicate measurements of fluid samples from the experiments indicate an uncertainty of the reported $pH_{(25\ °C)}$ value of ±0.02 units.

Mineral products were retrieved from both experiments when the runs were terminated after 78 days and 5 days. A variety of microscopic and analytical techniques were used to characterize solid reactants and experimental products, including XRD, EMPA, SEM, HRTEM, and XPS. Powder XRD analysis was carried out using a PANalytical X'Pert PRO Theta–Theta multipurpose diffractometer, equipped with a Cu anode operated at 45 kV and 40 mA, a divergent beam monochromator, and an X'Celerator detector. The scanning angle (2θ) ranged from 10.010 to 99.968°, with scan steps of 0.033°. Secondary minerals were analyzed on zero background quartz plate.

The chemical composition of alkali-feldspar lamellae (Table 1) was determined by wavelength dispersive EMPA using a CAMECA SX50. Operation accelerating voltage was 15 kV, while beam current and beam size were 15 nA and 1 μm, respectively. The structural

Table 1
Electron microprobe analysis (EMPA) results[a] of Na-rich laminae, K-rich laminae and whole alkali-feldspar grains

	Oxide	SiO_2	Al_2O_3	Na_2O	K_2O	FeO	CaO	Total
Na-rich laminae	wt.%	68.20	20.45	10.49	0.18	0.09	0.83	100.22
	S.D.[b]	0.03	0.05	0.18	0.06	0.03	0.04	
	N[c]	2.96	1.04	0.95	0.01	0.00	0.04	5.00
	S. D.	0.00	0.00	0.02	0.00	0.00	0.00	
K-rich laminae	wt.%	63.69	18.95	1.66	13.82	0.05	0.00	98.16
	S.D.	0.53	0.25	0.42	0.87	0.04	0.00	
	N	2.96	1.04	0.15	0.85	0.00	0.00	5.00
	S.D.	0.01	0.01	0.04	0.05	0.00	0.00	
Alkali-feldspar	wt.%	64.71	19.91	3.17	12.21			
	N	2.95	1.07	0.28	0.71			

[a] Each result reflects the average value of 5–10 measurements.
[b] S.D. = Standard deviation.
[c] *N* = the number of cations per 8 oxygen atoms.

formula for K-rich and Na-rich phases based on 8 oxygens is $K_{0.85}Na_{0.15}Al_{1.04}Si_{2.96}O_8$ and $K_{0.01}Na_{0.95}Ca_{0.04}Al_{1.04}Si_{2.96}O_8$, respectively.

SEM analysis was conducted with a Quanta 400 Field Emission Gun (FEG). The Energy Dispersive X-ray Spectrometer (EDS) system has an EDAX thin window and CDU LEAP detector. The low energy X-ray detection with FEG provided high spatial resolution for microanalysis down to ~0.1 μm^2.

A JEOL 1010 transmission electron microscope operated at 100 kV and a JEOL 2100F FEG Scanning Transmission Electron Microscope (STEM) with attached X-ray EDS and Gatan Imaging Filtering (GIF) system were used for analysis of reaction products. Thus, a fraction of the reaction products was immersed in ethanol and ultrasonically treated for several minutes. A small aliquot of the resulting suspension was mounted on a strip of holey-carbon film supported by a standard Cu TEM grid, prior to air-drying for approximately 10 min.

In addition to detailed examination of the fresh and reacted alkali-feldspar using microscopy, XPS was also used to determine the surface chemistry of the feldspar before and after hydrothermal reaction. XPS spectra of mineral reactant and products from the 78-day experiment were collected on a Physical Electronics 5400 instrument, with non-monochromatic Mg Kα as the X-ray source, operated at 300 W. Similar analyses from the 5-day experiment were collected on a PHI 5600ci instrument. This instrument made use of monochromatic Al Kα as the X-ray source, operated at 400 W. In both cases, mineral samples were embedded on double-sided adhesive tape, which was then fixed to the sample holder of the respective instruments. The samples were degassed at 10^{-7} Torr, before achieving operating vacuum at 5×10^{-8} Torr. The analysis area was 1 mm by 1.414 mm, while the photoelectron take-off angle was 45°. Survey scans (0–1200 eV binding energy) were performed first to determine the near-surface composition of the samples, followed by multiple repetitive scans over the energy regions of interest: Si_{2p}, O_{1s}, $K_{2p3/2}$ and Al_{2p}. Charge shifting of the analyzed photoelectrons was corrected by referencing a coexisting C_{1s} peak to 285.0 eV. Surface compositions of elements of interest were determined by analysis of peak areas taking explicit account of element specific atomic sensitivity factors.

Equilibrium constants for aqueous speciation calculations of fluid samples from experiments were calculated using a modified version of SUPCRT92 (Johnson et al., 1992). This code takes explicit account of recent revisions in keeping with the modified HKF equations of state for aqueous species (Shock and Helgeson, 1988; Shock et al., 1997; Sverjensky et al., 1997). Thermodynamic data for Al-bearing aqueous species, however, were from Tagirov and Schott (2001), while experimental data from Ho et al. (2001), Ho et al. (2000), and Ho et al. (1994) were used for $HCl_{(aq)}^{\circ}$, $KCl_{(aq)}^{\circ}$, and $NaCl_{(aq)}^{\circ}$, respectively. In practice, calculations needed to assess mineral saturation states, $pH_{(in\ situ)}$ (see below), and derive ion-activity diagrams were performed using the EQ3/6 computer code (Wolery and Daveler, 1992). Standard state thermodynamic properties for all Al-bearing minerals were from Holland and Powell (1998).

3. Results

3.1. Cations, anions and dissolved SiO_2

Time series changes in fluid chemistry from both experiments are listed in Table 2 and illustrated in Fig. 1. As anticipated from the relative abundances of fluid and mineral components used for the experiments, dissolved Cl^- concentrations remained relatively constant. The concentration of dissolved K^+, however, tended to decrease, although the extent of this represents a small fraction of that initially available in the fluid (200 mmol/kg).

Changes in dissolved concentrations of Na^+, Ca^{2+}, Al^{3+} and SiO_2 during the 78-day experiment were significant as alkali-feldspar dissolution proceeded. For example, dissolved SiO_2 increased slowly to approximately 1.70 mmol/kg after 456 h of reaction, then, surprisingly, decreased to 1.35 mmol/kg during the next 360 h of reaction, before again increasing to 4.18 mmol/kg at 1368 h. During the remaining 504 h of the experiment, dissolved SiO_2 decreased by 0.43 mmol/kg to a final value of 3.75 mmol/kg (Table 2). Dissolved concentrations of Na^+ and Ca^{2+} generally tracked with SiO_2, suggesting the possible involvement of non-stoichiometric dissolution of minor accessory components in albite in the moderately acidic fluids. Al^{3+} concentration decreased sharply during the first 216 h, then increased to 0.08 mmol/kg by 456 h before decreasing gradually throughout the remainder of the experiment. Dissolved concentrations of Na^+, Ca^{2+}, Al^{3+} and SiO_2 from the 5-day experiment at 120 h were largely consistent with changes in fluid chemistry of the 78-day experiment at a similar time of reaction (Fig. 1).

Table 2
Time-dependent changes in the composition of major dissolved constituents in aqueous fluid coexisting with alkali-feldspar at 200 °C and 300 bars

Sample #	Time	Cl^-	K^+	SiO_2	Na^+	Ca^{2+}	Al^{3+}	pH	*In situ* pH
	H	mmol/kg						25 °C	200 °C
78-day experiment									
	0	198.3	204.0	–	–	3.72	–	3.0	3.1
1	24	197.5	202.8	0.31	0.42	0.12	0.01	3.2	3.3
2	216	198.7	201.1	1.46	1.13	0.21	0.003	3.5	3.6
3	456	196.8	197.8	1.70	2.04	0.43	0.08	4.1	3.7
4	816	197.9	204.3	1.35	1.86	0.16	0.03	4.2	4.0
5	1368	199.5	197.0	4.18	3.72	0.30	0.01	4.9	4.5
6	1872	199.4	196.5	3.75	1.91	0.35	0.001	4.9	4.7
5-day experiment									
1	120	n.a.[a]	n.a.	1.31	0.88	0.35	0.005	n.a.	n.a.

[a] n.a. = not available.

3.2. pH

It is well known from results of numerous studies of reaction kinetics of silicate minerals in aqueous fluids that pH plays a particularly important role in the rate of mineral dissolution/precipitation processes. This is the case during the present study as well. To examine pH effects, the pH value measured for the fluid sample at ambient conditions (25 °C, 1 bar) (bench pH) was re-calculated at experimental conditions (200 °C, 300 bars) by taking account of the effect of temperature and pressure on the distribution of aqueous species. Accordingly, pH (*in situ*) was calculated for each sample taken during the course of experiments (Table 2). Owing to the relatively low experimental temperature, however, pH (*in situ*) was close to that measured, with an offset that ranged from approximately 0.1 to 0.4 units. During the 78-day experiment, pH values increased from 3.1 to 4.7 (Table 2).

3.3. Characterization of solid reactants and products

SEM photomicrographs of alkali-feldspar following the 78-day (Fig. 2A, B) and 5-day experiments (Fig. 2C, D) reveal channels and etch pits demonstrating dissolution heterogeneity, with albite lamellae preferentially dissolved. The presence of these mineral dissolution features was less obvious from results of the 5-day experiment.

Secondary minerals, with cross sectional diameter (d) of less than 0.5 μm and height (h) of approximately 0.1 μm, covered approximately 20% of total alkali-feldspar surface from the 78-day experiment. Alteration products also exhibited hexagonal shape. In the 5-day experiment, however, secondary minerals covered much less (~5%) of feldspar surface (Fig. 2). In both cases, secondary minerals were evenly distributed on the feldspar surface, suggesting no structural inheritance from the alkali-feldspar precursor. Feldspar dissolution and

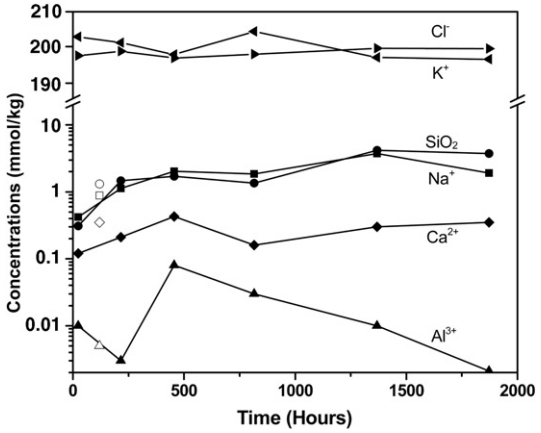

Fig. 1. Changes in the dissolved concentrations of selected aqueous constituents with time for the perthitic alkali-feldspar dissolution experiments at 200 °C and 300 bars. Dissolved concentrations of K^+, Cl^-, Na^+, Ca^{2+}, Al^{3+} and SiO_2 for the 78-day experiment (solid symbols) and Na^+, Ca^{2+}, Al^{3+} and SiO_2 for the 5-day experiment (open symbols). Time series changes for K^+, Cl^- concentrations for the 5-day experiment are not available beyond the start of the experiment (Table 2).

secondary mineral formation are likely coupled in the overall mass transfer process.

XRD patterns of mineral products in both experiments showed the presence of kaolinite as well as boehmite (Fig. 3A, B). The high peak intensities of boehmite in the XRD patterns likely result from preferential orientation of boehmite, and are not directly proportional to abundance.

Due to relatively low magnification of the JEOL 1010 operated at low voltage (100 kV), secondary mineral products (kaolinite and boehmite) from the 78-day experiment were manifest as a transparent phase with hexagonal shape and sizes of 200–300 nm (Fig. 4A). Selected area electron diffraction (SAED) patterns indicated that most alteration minerals are sheet silicates (Fig. 4B). The existence of boehmite crystals with rounded shapes, however, was confirmed by HRTEM observation with JEOL FEG 2100F (Fig. 4C). TEM images also showed "seesaw" edges of reacted alkali-feldspar from the experiment (Fig. 4D), suggesting preferential dissolution of Na lamellae, which is consistent with SEM observations. In the 5-day experiment, boehmite with distinctly sharp edges was observed on alkali-feldspar as the lone secondary mineral (Fig. 4E), which was confirmed by [010] SAED patterns, showing two dimensions for the Al octahedral structure (Fig. 4F). In contrast with boehmite from the 5-day experiment, boehmite following the 78-day experiment showed dissolution features characterized by more rounded grain boundaries (Fig. 4C).

Recently, Zhu et al. (2004a, 2006) observed an amorphous layer on naturally weathered feldspar, typically a few tens of nanometers thick. In the 78-day experiment, HRTEM observation also indicated that the alkali-feldspar grains were rimmed with an apparently amorphous layer (Fig. 4C). The amorphous nature of the edges was confirmed by the absence of electron diffraction pattern. It is still controversial whether an amorphous layer is caused by leaching (Nugent et al.,

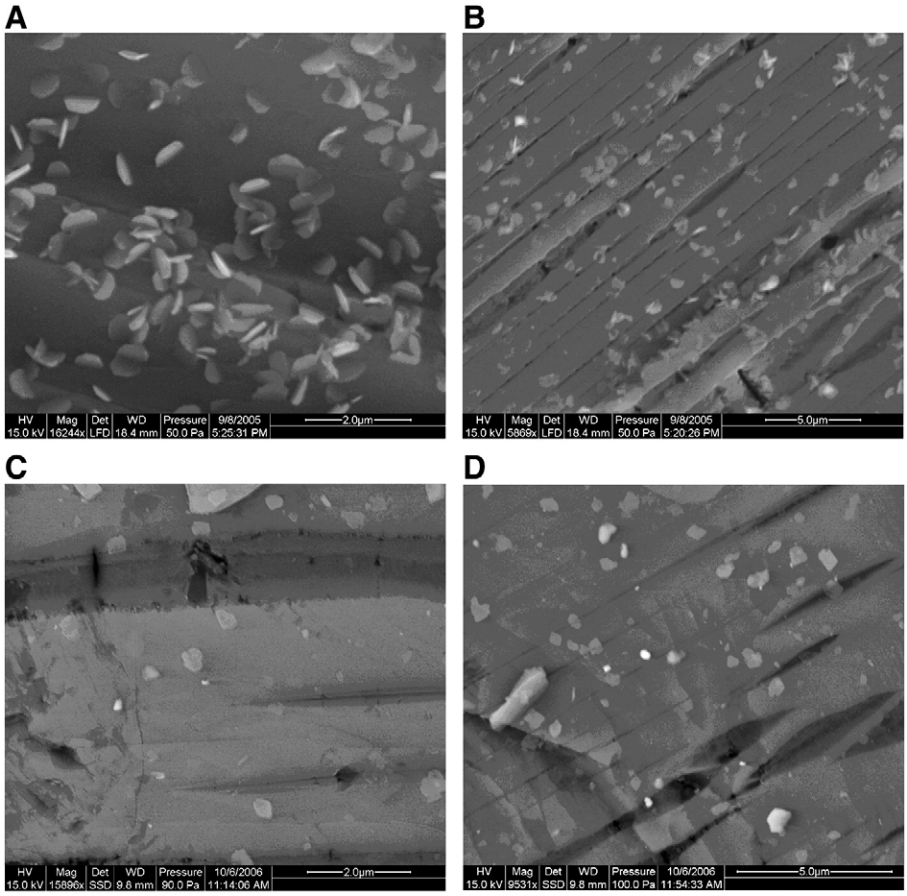

Fig. 2. SEM backscatter images of alkali-feldspar dissolution effects following reaction after 78 days (A, B) and 5 days (C, D). Reacted feldspar from the 78-day experiment reveal small (~0.5 µm) hexagon-shaped secondary minerals covering approximately 20% of the feldspar surface. In the 5-day experiment, secondary minerals cover only about 5% of the feldspar surface. The relative abundance of surface mineralization on the feldspars from each experiment is consistent with observed distribution of mineral dissolution features, such as laminar channels and etch pits on Na-rich lamina.

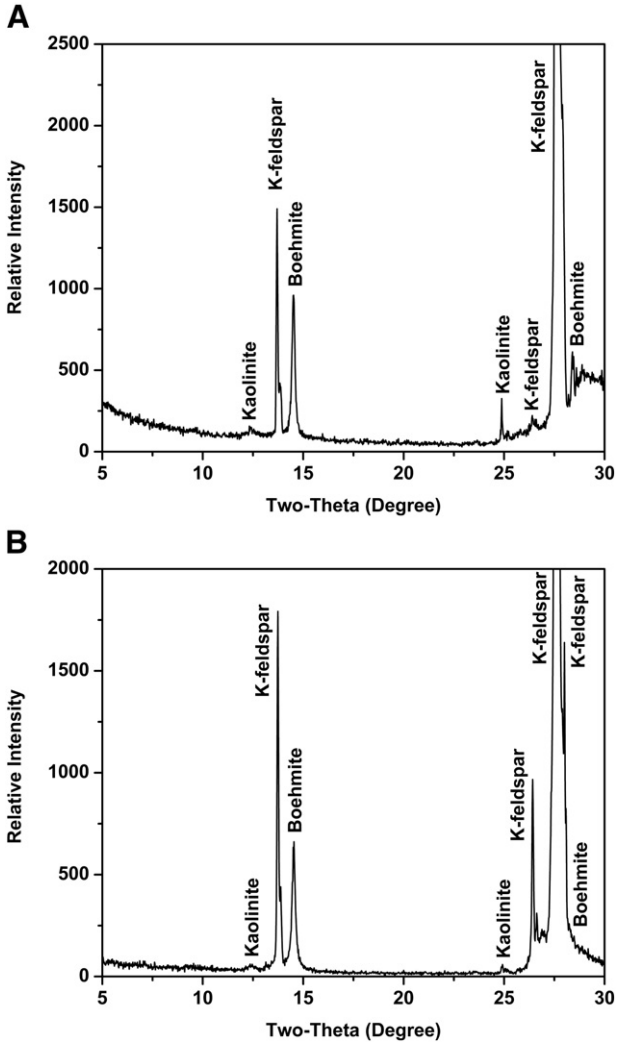

Fig. 3. X-ray diffraction patterns of mineral products following the 5-day experiment (A) and 78-day experiment (B). Kaolinite, boehmite, and K-feldspar were identified. The high peak intensity of boehmite is not a reflection of its abundance, but rather the result of preferential orientation.

1998; Nesbitt and Skinner, 2001) or is the result of silica reprecipitation effects (Hellmann et al., 2003, 2004).

Assuming that the majority of secondary minerals from the 78-day experiment are kaolinite (see below), we can estimate the abundance and surface area of this phase from dimensions determined from SEM examination. The surface area (s_{kln}) and volume (v_{kln}) of each kaolinite grain can be estimated geometrically assuming all crystals are hexagonal prisms, as follows:

$$s_{kln} = \frac{3\sqrt{3}}{2}\left(\frac{d}{2}\right)^2 \quad (1)$$

$$v_{kln} = s_{kln} \cdot h = \frac{3\sqrt{3}}{2}\left(\frac{d}{2}\right)^2 h. \quad (2)$$

Here we assume that the coverage (x) of kaolinite is ~20% of total alkali-feldspar surface area (normalized surface area ($SA_{alkali\text{-}feldspar}$) times mass ($m_{alkali\text{-}feldspar}$)). The number ($i$) of kaolinite grains produced by the end of the experiment is:

$$i = \frac{x \cdot SA_{alkali-feldspar} \cdot m_{alkali-feldspar}}{s_{kln}}. \quad (3)$$

The abundance of kaolinite (m_{kln}) can be calculated as follows:

$$m_{kln} = i \cdot v_{kln} \cdot D_{kln} = x \cdot h \cdot SA_{alkali-feldspar} \cdot m_{alkali-feldspar} \cdot D_{kln} \quad (4)$$

where D_{kln} is the density of kaolinite (2.594 g/cm^3). Thus, it follows that the normalized surface area of kaolinite is:

$$SA_{kln} = \frac{x \cdot SA_{alkali-feldspar} \cdot m_{alkali-feldspar}}{m_{kln}} \quad (5)$$

or

$$SA_{kln} = \frac{1}{h \cdot D_{kln}}. \quad (6)$$

Calculations indicate that at the end of the 78-day experiment, 10 mg of kaolinite was produced, with a surface area of approximately 3.86 m^2/g.

XPS data for the alkali-feldspar before the 78-day experiment indicate K/Al and Al/Si mole ratios of 0.66 and 0.37, respectively. These data are in good agreement with the surface chemistry of the fresh feldspar used for the 5-day experiment in spite of the fact that two different instruments were utilized to acquire the data (Table 3). Following the 78-day experiment, however, the Al/Si mole ratio increased significantly to 0.57, while K/Al decreased to 0.37. These data confirm the existence of secondary mineral phases, such as kaolinite and boehmite, where Al has a greater compositional percentage than for K-feldspar or albite. Results from the 5-day experiment also indicate an increase of Al/Si mole ratio to 0.41, while the K/Al remained constant at 0.61, which can best be accounted for by formation of aluminous secondary minerals, but in less abundance than for the 78-day experiment.

4. Discussion

4.1. Albite dissolution

Based on distribution of aqueous species calculations at experimental conditions, mineral saturation states during the experiments were determined (Table 4). The calculated saturation indices (SI, SI = log Q/K) indicate that throughout the experiments, the SI of albite is always negative, whereas the SI of K-feldspar becomes positive between 216 and 456 h of reaction (78-day experiment). Therefore, albite hydrolysis is predicted to occur throughout the experiment, while K-feldspar incrementally approaches saturation and then supersaturation. This is consistent with SEM and TEM observations of mineral products showing preferential dissolution of Na lamellae during the study (Figs. 2 and 4D), an observation consistent with results of earlier studies (Busenburg and Clemency, 1976; Lagache, 1976; Bevan and Savage, 1989; Rafal'skiy et al., 1990; Lee and Parsons, 1995; Tsuchiya et al., 1995).

4.1.1. General compositional trend

Albite hydrolysis can be illustrated by the following reaction:

$$\underset{NaAlSi_3O_8}{\text{Albite}} + H^+ + 0.5H_2O = 0.5\,\underset{Al_2Si_2O_5(OH)_4}{\text{Kaolinite}} + Na^+ + 2SiO_2(aq). \quad (7)$$

Thus, dissolution of albite releases SiO_2 and Na^+ into solution by consuming H^+. In a batch reactor, the concentrations of dissolved SiO_2 and Na^+ will increase, while H^+ decreases. Accordingly, time series observations of the changes in the ratio of log $a Na^+/a H^+$ versus log $aSiO_{2(aq)}$ provide a means to qualitatively assess mineral reactions within a broader context of congruency and incongruency involving phase relations in the Na_2O–Al_2O_3–SiO_2–H_2O–HCl system (Fig. 5A).

Experimental data involving dissolution of numerous aluminosilicate minerals often reveal incongruency as reflected by the

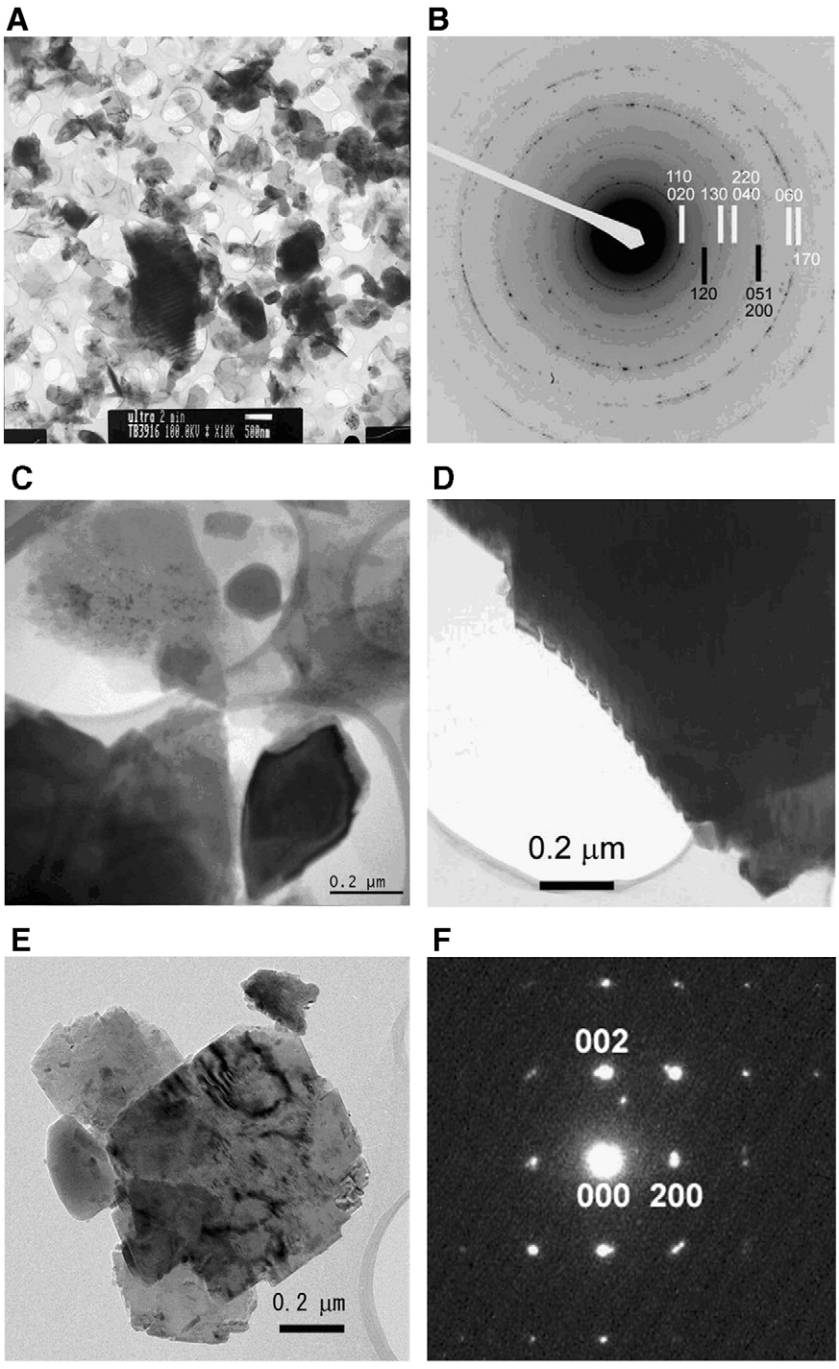

Fig. 4. TEM images and SAED patterns of mineral products from alkali-feldspar dissolution experiments at 200 °C and 300 bars. (A) Feldspar (large grains) and hexagonal secondary minerals (200–300 nm sized grains); (B) SAED pattern of mineral products labeled with Miller Indices for kaolinite (upper layer) and boehmite (lower layer); (C) Bright-field TEM image showing secondary minerals, with an alkali-feldspar grain at lower-right corner; (D) TEM image showing alkali-feldspar grain (dark color), seesaw edges indicate preferential dissolution of Na laminae; (E) TEM image showing alkali-feldspar grains with alteration mineral phases from the 5-day experiment; (F) [010] SAED pattern showing the octahedral structure of boehmite in the 5-day experiment. Unless otherwise noted, all samples were from the 78-day experiment. Image (A) was obtained by JEOL 1010 at 100 kV and (B)–(F) by JEOL 2100F at higher operating voltage.

nonstoichiometric release to solution of mineral components. This is most often caused by precipitation of secondary minerals or by preferential leaching of more reactive species in the primary mineral. The composition of the fluid coexisting with minerals undergoing dissolution will also affect the nonstoichiometric release of components (Amrhein and Suarez, 1988; Casey et al., 1988; Nesbitt and Muir, 1988; Hellmann et al., 1989, 1990; Inskeep et al., 1991; Nesbitt et al., 1991; Amrhein and Suarez, 1992; Alekseyev et al., 1993; Casey et al., 1993; Oxburgh et al., 1994; Stillings and Brantley, 1995; Gout et al., 1997; Brantley, 2003). The relatively acidic conditions (low $a\mathrm{Na}^+/a\mathrm{H}^+$) that characterized the starting fluid for the experiments, for example, initiated albite dissolution in the boehmite field of stability. Accordingly, early stage formation of boehmite is predictable (Fig. 5A), which can be illustrated as follows:

$$\underset{\mathrm{NaAlSi_3O_8}}{\text{Albite}} + \mathrm{H}^+ = \underset{\mathrm{AlO(OH)}}{\text{Boehmite}} + \mathrm{Na}^+ + 3\mathrm{SiO_2(aq)} \quad (8)$$

Subsequent compositional changes in solution progressed slowly toward the kaolinite field of stability (Fig. 5A). Indeed, fluid composition revealed by samples 3 and 4 during the 78 day

Table 3
XPS surface composition results[a] of alkali-feldspar from both experiments in comparison with theoretical values for K-feldspar and kaolinite

	K	Al	O	Si	K/Al	Al/Si
	mol%				Mole ratio	Mole ratio
Starting alkali-feldspar[b]	5.7	8.7	62.2	23.4	0.66	0.37
78-day experiment product	4.3	11.6	63.6	20.4	0.37	0.57
Starting alkali-feldspar[c]	4.8	7.9	63.2	24.1	0.61	0.33
5-day experiment product	5.5	9.0	63.4	22.1	0.61	0.41
K-feldspar	7.7	7.7	61.5	23.1	1	0.33
Kaolinite	–	20.9	55.8	21.8	–	1

[a] Each result reflects the average value of 4 measurements from different alkali-feldspar grains within the same sample.
[b] 78-day experiment.
[c] 5-day experiment.

experiment provide evidence for boehmite conversion to kaolinite as indicated by the decrease in dissolved silica, an overall process that can be illustrated as follows:

$$\underset{AlO(OH)}{\text{Boehmite}} + 0.5H_2O + SiO_2(aq) = 0.5\,\underset{Al_2Si_2O_5(OH)_4}{\text{Kaolinite}} \quad (9)$$

The calculated saturation indices for boehmite and kaolinite at 456 and 816 h of reaction, however, reflect supersaturation (Table 4). Apparently, the rate of albite dissolution is sufficient to maintain a level of supersaturation in spite of ongoing precipitation of both minerals, especially kaolinite.

As reactions proceed, compositional changes in the fluid (e.g., samples 5 and 6) indicate on-going dissolution of albite, which is likely accompanied by further replacement of boehmite by kaolinite, especially as increasing amounts of silica are dissolved. Thus, it is not surprising that the fluid pH increases (reactions (7) and (8)), although the rate of increase is surprisingly slow given the temperature of the experiment. That there is virtually no change in $a\mathrm{Na}^+/a\mathrm{H}^+$ and only 0.43 mmol/kg decrease in dissolved SiO_2 from sample intervals 5 to 6 (1369–1872 h of reaction) underscores the sluggishness of rates of mass transfer between metastable minerals (e.g., boehmite to kaolinite), even for high degrees of supersaturation ultimately caused by albite dissolution.

Prediction of reaction progress based on changes in fluid chemistry is generally consistent with mineral product analysis data. For example, in the 78-day experiment, XPS data indicate an increase in Al/Si mole ratio from 0.37 to 0.57 and a decrease in K/Al from 0.66 to 0.37, consistent with greater coverage by kaolinite on alkali-feldspar surfaces. These data are consistent with SEM and HRTEM observations. Moreover, TEM images show that for the 78-day experiment, boehmite takes on a rounded shape, which is consistent with constraints imposed by reaction (9). This is in contrast with the sharp edges of boehmite observed following the 5-day experiment.

4.1.2. Albite dissolution rate

The lack of dissolved Na^+ in the fluid used for the experiments together with the apparent lack of formation of Na mineralization during the course of the experiments permits time series changes in dissolved Na^+ to serve as a constraint on the rate of albite dissolution. This approach is of course limited by the well known $Na^+ \Leftrightarrow H_3O^+$ exchange reaction on the feldspar surface at the initial stage of the reaction (e.g., Helgeson et al., 1984), but the exchanged amounts remain to be constant in evaluation of the time series data (Alekseyev et al., 1997). Our experimental data indicate significant and continuous increase in dissolved Na^+ during the early stages of the experiments, although both the rate and magnitude of Na^+ gain decreases appreciably with reaction progress, especially beyond 500 h of reaction (Table 2). The lessening of the Na^+ flux is likely caused by the gradually diminishing thermodynamic drive for albite dissolution.

Taking account of the rate of release of dissolved Na^+ during the first 456 h of reaction of the 78-day experiment (Table 2) suggests albite dissolution rate of approximately 5.0×10^{-11} mol s^{-1}. This value is in good agreement with the rate of albite dissolution determined by Hellmann (1994) for a similar temperature, albite surface area, and mineral (albite)–fluid saturation state.

The apparent decrease in the rate of albite dissolution with reaction progress results from changes in solution chemistry that affects the driving force for the reaction (Lasaga, 1981; Aagaard and Helgeson, 1982; Helgeson et al., 1984; Nagy and Lasaga, 1992). The increase in pH that occurs with reaction progress (reactions (7) and (8)) can induce changes in composition and microtopography of the mineral (albite) surface (reactive surface area, etch pits) (Holdren and Speyer, 1985; Brantley et al., 1986; Holdren and Speyer, 1987; Casey et al., 1988; Schott et al., 1989; Blum and Lasaga, 1991; Amrhein and Suarez, 1992; Brady and Walther, 1992; Wollast and Chou, 1992; Oelkers et al., 1994), further inhibiting albite dissolution kinetics.

4.1.3. Coupled reaction processes

Time (t) dependent changes in dissolved SiO_2 can be used effectively to assess rates of incremental reaction steps in the overall mineral dissolution–reprecipitation processes during the 78-day experiment, as follows:

$$r = \frac{w\cdot\sum_{1}^{l}\frac{1}{c}\Delta m_{SiO_{2(aq)}}}{t} \quad (10)$$

where r is the release/uptake rate of dissolved SiO_2, w is the mass of water in solution (kg), $\Delta m_{SiO_{2(aq)}}$ is the absolute value of SiO_2 concentration change (mol/kg) for each mineral dissolution or precipitation reaction, c is stoichiometric factor of SiO_2 in the reaction, while l is the number of simultaneous reactions considered at each stage of the experiment.

During the earliest stages of the experiment (Fig. 5A), reaction (8) is assumed to account for the release of dissolved SiO_2. Therefore, the rate of release of SiO_2 from albite not only provides a measure of the dissolution rate of this mineral, but also the rate of formation of boehmite. For example, the change in dissolved SiO_2 during the first 456 h of reaction is 1.70 mmol/kg, which when normalized to the mass of fluid actually present, yields 6.80×10^{-5} mol. Accordingly, taking account of the stoichiometry depicted by reaction (8), the rates of albite dissolution and boehmite formation can be estimated to be 1.38×10^{-11} mol s^{-1} (Table 5). Although the rate of albite dissolution estimated by this method differs from that estimated earlier from the rate of Na^+ release, the two numbers are actually in good agreement considering uncertainties in mineral surface areas and composition, analytical uncertainties, and uncertainties related to the assumed conservation of dissolved Na^+ and $SiO_{2(aq)}$ at this stage in the overall reaction process.

Table 4
Changes of mineral saturation state (log Q/K) with time for alkali-feldspar dissolution experiments at 200 °C and 300 bars

Sample #	Time	Minerals				
	H	K-feldspar	Albite	Boehmite	Kaolinite	Muscovite
78-day experiment						
1	24	−2.82	−6.85	1.17	1.27	1.60
2	216	−0.82	−4.42	0.85	1.98	2.96
3	456	0.96	−2.38	2.34	5.10	7.73
4	816	0.68	−2.71	2.04	4.31	6.86
5	1368	2.00	−1.07	1.41	4.02	6.91
6	1872	1.40	−1.95	0.75	2.61	5.00
5-day experiment						
1	120	−1.14	−4.84	0.87	1.93	2.69

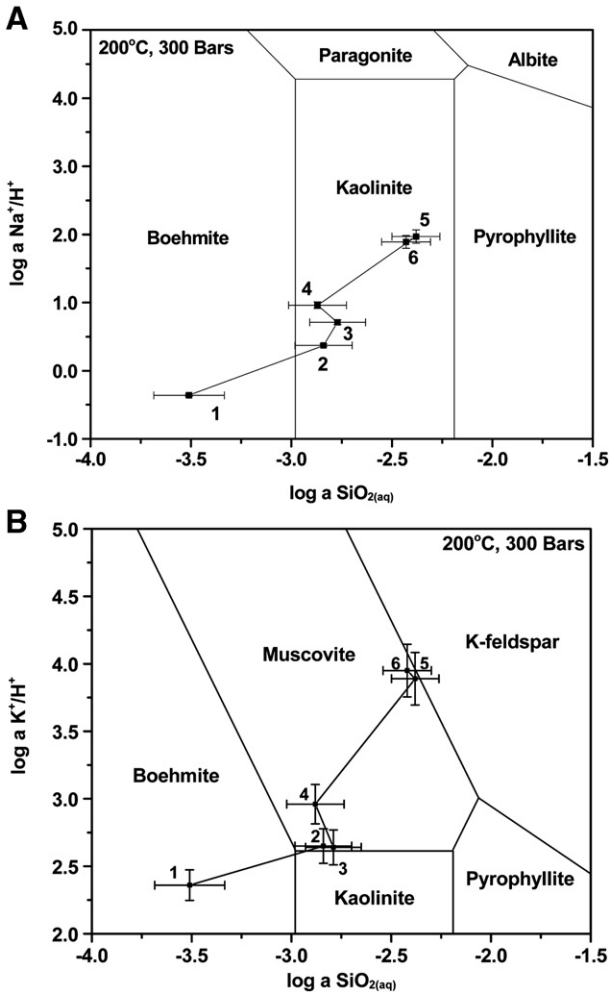

Fig. 5. Mineral phase diagrams in the Na_2O–Al_2O_3–SiO_2–H_2O–HCl (A) and K_2O–Al_2O_3–SiO_2–H_2O–HCl (B) system at 200 °C and 300 bars with experimental data showing time series change of $a\mathrm{Na}^+/a\mathrm{H}^+$ and $a\mathrm{K}^+/a\mathrm{H}^+$, respectively, with $a\mathrm{SiO}_2(\mathrm{aq})$ in alkali-feldspar dissolution experiment (78-day) at same conditions. The sizes of uncertainty bars for y axis (log $a\mathrm{Na}^+/a\mathrm{H}^+$) of samples 1–4 in (A) are smaller than the size of data symbols.

Using a similar approach for all reaction stages directly or indirectly contributing to the formation of kaolinite (Table 5), the mass of kaolinite formed throughout the experiment can be estimated to be approximately 11 mg. This value is similar to that estimated from SEM data, assuming all of the mineralization associated with the alkali-feldspar surface is kaolinite.

4.2. K-feldspar dissolution and precipitation

As shown above, K-feldspar was undersaturated before 456 h of reaction (Table 4). The dissolution of K-feldspar in moderately acidic aqueous fluid can be illustrated as follows:

$$\underset{3\mathrm{KAlSi_3O_8}}{\text{K – feldspar}} + 2\mathrm{H}^+ = \underset{\mathrm{KAl_3Si_3O_{10}(OH)_2}}{\text{Muscovite}} + 2\mathrm{K}^+ + 6\mathrm{SiO_2(aq)}. \quad (11)$$

Accordingly, dissolution of K-feldspar releases SiO_2 and K^+ into solution by consuming H^+ until K-feldspar–muscovite equilibrium is achieved. Owing to constraints imposed by temporal changes in fluid chemistry, data indicate that K-feldspar approached saturation and then supersaturation between 216 and 456 h of reaction, respectively (Table 4). Thus, subsequent to 456 h of reaction, K-feldspar dissolution is inhibited.

In the first 456 h of 78-day experiment, the relatively low fluid pH can be expected to enhance boehmite formation (Fig. 5B), as follows:

$$\underset{\mathrm{KAlSi_3O_8}}{\text{K – feldspar}} + \mathrm{H}^+ = \underset{\mathrm{AlO(OH)}}{\text{Boehmite}} + \mathrm{K}^+ + 3\mathrm{SiO_2(aq)}. \quad (12)$$

As emphasized previously, kaolinite was the dominant alteration mineral product to form during the 78-day experiment owing to the preferential reactivity of albite. Data indicate, however, a large (−21.76 kJ/mol) thermodynamic drive to convert kaolinite to muscovite in a manner consistent with the following reaction:

$$\underset{3\mathrm{Al_2Si_2O_5(OH)_4}}{\text{Kaolinite}} + 2\mathrm{K}^+ = \underset{2\mathrm{KAl_3Si_3O_{10}(OH)_2}}{\text{Muscovite}} + 2\mathrm{H}^+ + 3\mathrm{H_2O}. \quad (13)$$

The end of the 78-day experiment did not achieve K-feldspar–muscovite–fluid equilibria. Instead, the system is at a metastable state as suggested by the coexistence of kaolinite and K-feldspar, and the apparent absence of muscovite in spite of a strong thermodynamic drive for its formation (Table 4). Similar observations have long been reported based on field and experimental studies of hydrothermal and diagenetic systems (Huang et al., 1986; Ehrenberg, 1991; Bjørlykke and Aagaard, 1992; Ehrenberg et al., 1993).

The experimental results by Huang et al. (1986) depicting conversion of albite to illite showed that the formation of illite occurred most effectively under near neutral pH conditions, while boehmite and kaolinite were formed in initially acidic solution. Moreover, kinetic modeling conducted by Berger et al. (1997) showed that the energy barrier for kaolinite conversion to illite is greater than 8.4 kJ/mol at 120 °C, which helps to explain kaolinite metastability. Similarly in the 78-day experiment, the relatively acidic fluid chemistry initiated albite dissolution in the boehmite stability field (Fig. 5A), which resulted in early formation of boehmite, followed by kaolinite. Although muscovite formation by reaction (13) is increasingly thermodynamically favored with reaction progress (Table 4), with Gibbs free energy of −21.76 kJ/mol at 1872 h of reaction, kaolinite persists, while muscovite or illite failed to form in detectable amounts.

Theoretical calculations (Berger et al., 1997) and experimental data (Huang et al., 1986) indicate that changes in fluid chemistry, such as consumption of H^+ or increase in K^+, facilitate conversion of kaolinite to muscovite, which is consistent with the relatively high $a\mathrm{K}^+/a\mathrm{H}^+$ values for muscovite stability (Table 4; Fig. 5B). Using a rate law and rate constant (2.74×10^{-12} kg m^{-2} s^{-1}) proposed by Chermak and Rimstidt (1990), which explicitly accounts for constraints imposed by fluid chemistry, we can obtain a provisional estimate of the conversion rate of kaolinite to muscovite. These data indicate that approximately 189 days beyond the time of sample 6 (78 days) would be required to convert all of the kaolinite (10 mg) with an inferred surface area of 3.86 m^2/g to muscovite (reaction (13)). The accuracy of this prediction is constrained by the fact that it is not possible to explicitly account for

Table 5
Reaction stages in alkali-feldspar dissolution experiment, and corresponding key reactions and corresponding mineral dissolution/precipitation rates[a]

Stage	Samples	Time	Key reactions	Reaction rates (mol s^{-1})	
		H		Dissolution	Precipitation
1	1–3	0–456	$NaAlSi_3O_8+H^+=AlO(OH)+Na^++3SiO_{2(aq)}$	1.38×10^{-11} (*Ab*)	1.38×10^{-11} (*Bmt*)
2	3–4	457–816	$AlO(OH)+0.5H_2O+SiO_{2(aq)}=0.5Al_2Si_2O_5(OH)_4$	1.08×10^{-11} (*Bmt*)	5.40×10^{-12} (*Kln*)
3	4–5	817–1368	$NaAlSi_3O_8+H^++0.5H_2O=0.5Al_2Si_2O_5(OH)_4+Na^++2SiO_{2(aq)}$	2.85×10^{-11} (*Ab*)	1.42×10^{-11} (*Kln*)
4	5–6	1369–1872	$AlO(OH)+0.5H_2O+SiO_{2(aq)}=0.5Al_2Si_2O_5(OH)_4$	9.48×10^{-12} (*Bmt*)	4.74×10^{-12} (*Kln*)

Ab: albite; *Bmt*: boehmite; *Kln*: kaolinite.
[a] The dissolution/precipitation rates were calculated based on the predominant reaction controlling dissolved SiO_2 changes in each stage.

the full effects of subsequent changes in fluid chemistry and effective surface area that will influence mineral dissolution (albite) and precipitation (muscovite) processes. A more serious limitation, however, involves the complete lack of data intrinsic to muscovite nucleation and growth. It is well known, for example, that the rate of mineral nucleation is controlled by interfacial energy, the collision frequency efficiency, temperature, as well as supersaturation (Nielsen, 1986). In the absence of these data, the provisional rate for kaolinite conversion to muscovite estimated above must be taken as a minimum value.

Between 216 and 456 h of reaction, K-feldspar became supersaturated. Other than alkali-feldspar microtextural control (Lee and Parsons, 1995), the high K^+ concentration of the starting fluid undoubtedly plays a role in the observed reaction path processes as well. For example, the high concentration of dissolved K^+ in the starting fluid (200 mmol/kg), together with constraints imposed by the coexistence of two alkali feldspars, provide ample driving force for the reaction between these two feldspars to proceed as follows:

$$\underset{NaAlSi_3O_8}{\text{Albite}} + K^+ = \underset{KAlSi_3O_8}{\text{K}-\text{feldspar}} + Na^+. \quad (14)$$

Calculations indicate that the Gibbs free energy change for the above reaction at 200 °C, 300 bars varies from −31.67 to −22.97 kJ/mol. Accordingly, as reactions proceed, the concentrations of dissolved K^+ and Na^+ are predicted (and observed) to decrease and increase, respectively. In detail, however, the "cation exchange" reaction between albite and K-feldspar is an exceedingly complex process, involving breakdown and rebuilding of Si–O and Al–O bonds (O'Neil and Taylor, 1967; O'Neil, 1977) and dissolution and precipitation with an abrupt discontinuity at the interface (Labotka et al., 2004). The possible rimming of K-feldspar on the albite component undoubtedly limits reaction rates and extent of mass transfer on the time scale of the experiment.

4.3. Coupled dissolution and precipitation reaction kinetics

In the absence of precipitation of muscovite/illite during the present experiments, the build up of solutes would provide a negative feedback on the rate of dissolution of the primary feldspars. This has important implications for the application of chemical kinetics to natural systems, as emphasized by Lasaga (1998). Lasaga (1998) showed a series of scenarios of possible reaction paths with different ratios of rate constants between feldspar and secondary clay mineral products. Indeed, results show that the dissolution rate of primary feldspar is an explicit function of the relative rates of all irreversible reactions in the system. In cases where the ratio of the reaction rate constant of secondary minerals to that of feldspar dissolution is small (as might be the case during the present experiment), the metastable coexistence of Al hydroxide and kaolinite grows significantly. At a sufficiently small value it is possible that three alteration phases including muscovite, could coexist with the primary feldspar. Thus, reaction path models based on assumptions of partial equilibria that necessarily entail formation of chemically complex secondary phases immediately upon saturation of the fluid with respect to these minerals will provide uncertain constraints on the chemical evolution of fluids and minerals in time and space in hydrologic and even hydrothermal systems.

5. Conclusions

Alkali-feldspar hydrolysis experiments using a well-mixed batch reactor allowed observations of time series *in situ* fluid chemistry at 200 °C and 300 bars to be integrated with the mineralogy and composition of reaction products retrieved after 5 and 78 days. Hydrolysis of the albite component of alkali-feldspar resulted in the formation of boehmite, and then kaolinite. SEM, HRTEM and XPS analyses of the surface of alkali-feldspar provide clear evidence for the preferential reaction of albite and coexistence of secondary mineralization involving both boehmite and kaolinite. The experimentally observed release of Na^+ and $SiO_{2(aq)}$ during the earliest stages of reaction of the 78-day experiment (less than 500 h) indicate a dissolution rate for albite in agreement with other studies when mineral surface area, temperature and saturation state effects are taken into account. The rate of albite dissolution becomes slower during late stages of reaction, likely due to the formation of secondary minerals on active sites on the albite surface and/or the gradually diminished thermodynamic drive for albite dissolution. The metastable existence of kaolinite results in part from intrinsically sluggish conversion of kaolinite to muscovite in moderately acidic fluids.

Traditionally, feldspar hydrolysis is treated with the assumption of partial equilibria between the secondary minerals and the aqueous solution. If this partial equilibrium is not observed, the reaction paths are different in terms of both aqueous solution chemistry and secondary mineral paragenesis (Lasaga, 1998). Our detailed mineralogical analysis showed that boehmite and kaolinite persisted metastably during the entire 78 days experiment, which provides the first experimental evidence to support early modeling illustrations (Steefel and van Cappellen, 1990; Lasaga, 1998). The time series solution chemistry data and calculated saturation indices are also more consistent with Lasaga's (1998) cases with slow clay precipitation kinetics than the partial equilibrium case. Slow secondary mineral reaction kinetics means strong coupling between dissolution and precipitation reactions, which is important in interpretation of field derived rates (Zhu et al., 2004a,b).

Acknowledgments

Material in this paper is based upon work supported by the U.S. Department of Energy under Award No. DE-FG26-04NT42125 to CZ and WES and partially by the National Science Foundation under Award No.'s EAR0423971 and EAR0509775 to CZ. Any opinions, findings, and conclusions or recommendations expressed in this material, however, are those of the authors and do not necessarily reflect the views of the United States Government or any agency thereof. We thank Rick Haasch and John Baltrus for assistances with XPS analyses that were carried out in the Center for Microanalysis of Materials, University of Illinois and the National Energy Technology Laboratory. We thank Rick Knurr at University of Minnesota for chemical analyses of fluid samples, and Kyle Jones at US EPA for BET surface analysis. We also thank Arndt Schimmelmann at Indiana University for helping with techniques in sample preparation protocols and Sheila Hedges at NETL for reading an earlier version of the manuscript. The paper greatly benefited from comments and suggestions made by John Kaszuba as well as comments from an anonymous reviewer and editor Jeremy Fein.

References

Aagaard, P., Helgeson, H.C., 1982. Thermodynamic and kinetic constraints on reaction rates among minerals and aqueous solutions: I. Theoretical considerations. American Journal of Science 282, 237–285.

Alekseyev, V.A., Prisyagina, N.I., Medvedeva, L.S., 1993. Rates of congruent dissolution of feldspars in acid and alkaline hydrothermal solutions. Geochemistry International 30, 26–35.

Alekseyev, V.A., Medvedeva, L.S., Prisyagina, N.I., Meshalkin, S.S., Balabin, A.I., 1997. Change in the dissolution rates of alkali feldspars as a result of secondary mineral precipitation and approach to equilibrium. Geochimica et Cosmochimica Acta 61, 1125–1142.

Amrhein, C., Suarez, D.L., 1988. The use of a surface complexation model to describe the kinetics of ligand-promoted dissolution of anorthite. Geochimica et Cosmochimica Acta 52, 2785–2793.

Amrhein, C., Suarez, D.L., 1992. Some factors affecting the dissolution kinetics of anorthite at 25 °C. Geochimica et Cosmochimica Acta 56, 1815–1826.

Berger, G., Lacharpagne, J.-C., Velde, B., Beaufort, D., Lanson, B., 1997. Kinetic constraints on illitization reactions and the effects of organic diagenesis in sandstone/shale sequences. Applied Geochemistry 12, 23–35.

Bevan, J., Savage, D., 1989. The effect of organic acids on the dissolution of K-feldspar under conditions relevant to burial diagenesis. Mineralogical Magazine 53, 415–425.
Bjørlykke, K., Aagaard, P., 1992. Clay minerals in North Sea sandstones. Origin, Diagenesis, and Petrophysics of Clay Minerals in Sandstones. SEPM Special Publication, vol. 47, pp. 65–80.
Blum, A.E., Lasaga, A.C., 1991. The role of surface speciation in the dissolution of albite. Geochimica et Cosmochimica Acta 55, 2193–2201.
Brady, P.V., Walther, J.V., 1992. Surface chemistry and silicate dissolution at elevated temperatures. American Journal of Science 292, 639–658.
Brantley, S.L., 2003. Reaction kinetics of primary rock-forming minerals under ambient conditions. In: Drever, J.I. (Ed.), Surface and Ground Water, Weathering, and Soils. Holland, H.D., Turekian, K.K. (Eds.), Treatise on Geochemistry, Vol. 5, Pergamon Press, Oxford, 73–117.
Brantley, S.L., Stillings, L.L., 1996. Feldspar dissolution at 25 °C and low pH. American Journal of Science 296, 101–127.
Brantley, S.L., Crane, R., Crerar, D.A., Hellman, R., Stallard, R., 1986. Dislocation etch pits in quartz. In: Davis, J., Hayes, K. (Eds.), Geochemical Processes at Mineral Surfaces. American Chemical Society, pp. 639–649.
Burch, T.E., Nagy, K.L., Lasaga, A.C., 1993. Free energy dependence of albite dissolution kinetics at 80 °C and pH 8.8. Chemical Geology 105, 137–162.
Busenburg, E., Clemency, C.V., 1976. The dissolution kinetics of feldspars at 25 °C and 1 atm CO2, partial pressure. Geochimica et Cosmochimica Acta 40, 41–49.
Casey, W.H., Westrich, H.R., Arnold, G.W., 1988. Surface chemistry of labradorite feldspar reacted with aqueous solutions at pH=2, 3 and 12. Geochimica et Cosmochimica Acta 52, 2795–2807.
Casey, W.H., Westrich, H.R., Banfield, J.F., Ferruzzi, G., Arnold, G.W., 1993. Leaching and reconstruction at the surfaces of dissolving chain-silicate minerals. Nature 366, 253–256.
Chermak, J.A., Rimstidt, J.D., 1990. The hydrothermal transformation rate of kaolinite to muscovite/illite. Geochimica et Cosmochimica Acta 54, 2979–2990.
Chou, L., Wollast, R., 1985. Steady-state kinetics and dissolution mechanisms of albite. American Journal of Science 285, 963–993.
Ehrenberg, S.N., 1991. Kaolinized, potassium-leached zones at the contacts of the Garn Formation, Haltenbanken, mid-Norwegian continental shelf. Marine and Petroleum Geology 8, 250–269.
Ehrenberg, S.N., Aagaard, P., Wilson, M.J., Frazer, A.R., Duthie, D.M.L., 1993. Depth-dependent transformation of kaolinite to dickite in sandstones of the Norwegian continental shelf. Clay Minerals 28, 325–352.
Gautier, J.M., Oelkers, E.H., Schott, J., 1994. Experimental study of K-feldspar dissolution rates as a function of chemical affinity at 150 °C and pH 9. Geochimica et Cosmochimica Acta 58, 4549–4560.
Gout, R., Oelkers, E.H., Schott, J., Zwick, A., 1997. The surface chemistry and structure of acid-leached albite: new insights on the dissolution mechanisms of the alkali feldspars. Geochimica et Cosmochimica Acta 61, 3013–3018.
Helgeson, H.C., 1968. Evaluation of irreversible reactions in geochemical processes involving minerals and aqueous solutions — I. Thermodynamic relations. Geochimica et Cosmochimica Acta 32, 853–877.
Helgeson, H.C., 1971. Kinetics of mass transfer among silicates and aqueous solutions. Geochimica et Cosmochimica Acta 35, 421–469.
Helgeson, H.C., 1972. Kinetics of mass transfer among silicates and aqueous solutions: correction and clarification. Geochimica et Cosmochimica Acta 36, 1067–1070.
Helgeson, H.C., 1974. Chemical interaction of feldspar and aqueous solutions. In: MacKenzie, W.S., Zussman, J. (Eds.), The Feldspars. Crane, Russak and Co. Inc., New York.
Helgeson, H.C., 1979. Mass transfer among minerals and hydrothermal solutions. In: Barnes, H.L. (Ed.), Geochemistry of Hydrothermal Ore Deposits. John Wiley & Sons, New York.
Helgeson, H.C., Garrels, R.M., Mackenzie, F.T., 1969. Evaluation of irreversible reactions in geochemical processing involving minerals and aqueous solutions — II. Applications. Geochimica et Cosmochimica Acta 33, 455–481.
Helgeson, H.C., Brown, T.H., Nigrini, A., Jones, T.A., 1970. Calculation of mass transfer in geochemical processes involving aqueous solutions. Geochimica et Cosmochimica Acta 34, 569–592.
Helgeson, H.C., Murphy, W.M., Aagaard, P., 1984. Thermodynamic and kinetic constraints on reaction rates among minerals and aqueous solutions: II. Rate constants, effective surface area, and the hydrolysis of feldspar. Geochimica et Cosmochimica Acta 48, 2405–2432.
Hellmann, R., 1994. The albite–water system: Part I. The kinetics of dissolution as a function of pH at 100, 200, and 300 °C. Geochimica et Cosmochimica Acta 58, 595–611.
Hellmann, R., 1995. The albite–water system: Part II. The time evolution of the stoichiometry of dissolution as a function of pH at 100, 200, and 300 °C. Geochimica et Cosmochimica Acta 59, 1669–1697.
Hellmann, R., Tisserand, D., 2006. Dissolution kinetics as a function of the Gibbs free energy of reaction: an experimental study based on albite feldspar. Geochimica et Cosmochimica Acta 70, 364–383.
Hellmann, R., Crerar, D.A., Zhang, R., 1989. Albite feldspar hydrolysis to 300 °C. Solid State Ionics 32/33, 314–329.
Hellmann, R., Eggleston, C.M., Hochella Jr., M.F., Crerar, D.A., 1990. The formation of leached layers on albite surfaces during dissolution under hydrothermal conditions. Geochimica et Cosmochimica Acta 54, 1267–1281.
Hellmann, R., Penisson, J.-M., Hervig, R.L., Thomassin, J.-H., Abrioux, M.-F., 2003. An EFTEM/HRTEM high-resolution study of the near surface of labradorite feldspar altered at acid pH: evidence for interfacial dissolution–reprecipitation. Physics and Chemistry of Minerals 30, 192–197.
Hellmann, R., Penisson, J.-M., Hervig, R.L., Thomassin, J.-H., Abrioux, M.-F., 2004. Chemical alteration of feldspar: a comparative study using SIMS and HRTEM/EFTEM. In: Wanty, R.B., Seal, R.R. (Eds.), Proceedings of the 11th International Symposium on Water–Rock Interaction, Saratoga Springs, New York.
Ho, P.C., Palmer, D.A., Mesmer, R.E., 1994. Electrical conductivity measurements of aqueous sodium chloride solutions to 600 °C and 300 MPa. Journal of Solution Chemistry 23, 997–1018.
Ho, P.C., Bianchi, H., Palmer, D.A., Wood, R.H., 2000. Conductivity of dilute aqueous electrolyte solutions at high temperatures and pressures using a flow cell. Journal of Solution Chemistry 29, 217–235.
Ho, P.C., Palmer, D.A., Gruszkiewicz, M.S., 2001. Conductivity measurements of dilute aqueous HCl solutions to high temperatures and pressures using a flow-through cell. Journal of Physical Chemistry B 105, 1260–1266.
Holdren, G.R., Berner, R.A., 1979. Mechanism of feldspar weathering — I. Experimental studies. Geochimica et Cosmochimica Acta 43, 1161–1171.
Holdren, G.R., Speyer, P.M., 1985. pH dependent change in the rates and stoichiometry of dissolution of an alkali feldspar at room temperature. American Journal of Science 285, 994–1026.
Holdren, G.R., Speyer, P.M., 1987. Reaction rate–surface area relationships during the early stages of weathering. II. Data on eight additional feldspars. Geochimica et Cosmochimica Acta 51, 2311–2318.
Holland, T.J.B., Powell, R., 1998. An internally consistent thermodynamic data set for phases of petrological interest. Journal of Metamorphic Geology 16, 309–343.
Huang, W.L., Bishop, A.M., Brown, R.W., 1986. The effect of fluid/rock ratio on feldspar dissolution and illite formation under reservoir conditions. Clay Minerals 21, 585–602.
Inskeep, W.P., Nater, E.A., Bloom, P.R., Vandervoort, D.S., Erich, M.S., 1991. Characterization of laboratory weathered labradorite surfaces using X-ray photoelectron spectroscopy and transmission electron microscopy. Geochimica et Cosmochimica Acta 55, 787–800.
Johnson, J.W., Oelkers, E.H., Helgeson, H.C., 1992. SUPCRT92 — A software package for calculating the standard molal thermodynamic properties of minerals, gases, aqueous species, and reactions from 1 bar to 5000 bar and 0 °C to 1000 °C. Computational Geosciences 18 (7), 899–947.
Knauss, K.G., Wolery, T.J., 1986. Dependence of albite dissolution kinetics on pH and time at 25 °C and 70 °C. Geochimica et Cosmochimica Acta 50, 2481–2497.
Labotka, T.C., Cole, D.R., Fayek, M., Riciputi, L.R., Stadermann, F.J., 2004. Coupled cation and oxygen-isotope exchange between alkali feldspar and aqueous chloride solution. American Mineralogist 89, 1822–1825.
Lagache, M., 1976. New data on the kinetics of the dissolution of alkali feldspars at 200 °C in CO2 charged water. Geochimica et Cosmochimica Acta 40, 157–161.
Lasaga, A.C., 1981. Transition state theory. In: Lasaga, A.C., Kirkpatrick, R.J. (Eds.), Kinetics of Geochemical Processes. Reviews in Mineralogy, vol. 8, pp. 135–169.
Lasaga, A.C., 1998. Kinetic Theory in the Earth Sciences. Princeton University Press, Princeton.
Lee, M.R., Parsons, I., 1995. Microtextural controls of weathering of perthitic alkali feldspars. Geochimica et Cosmochimica Acta 59, 4465–4488.
Morey, G.W., Fournier, R.O., 1961. The decomposition of microcline, albite, and nepheline in hot water. American Mineralogist 46, 688–699.
Nagy, K.L., 1995. Dissolution and precipitation kinetics of sheet silicates. In: White, A.F., Brantley, S.L. (Eds.), Chemical Weathering Rates of Silicate Minerals, vol. 31. Mineralogical Society of America, Washington, DC, pp. 173–225.
Nagy, K.L., Lasaga, A.C., 1992. Dissolution and precipitation kinetics of gibbsite at 80 °C and pH 3: the dependence on solution saturation state. Geochimica et Cosmochimica Acta 56, 3093–3111.
Nagy, K.L., Blum, A.E., Lasaga, A.C., 1991. Dissolution and precipitation kinetics of kaolinite at 80 °C and pH 3: the dependence on solution saturation state. American Journal of Science 291, 649–686.
Nesbitt, H.W., Muir, I.J., 1988. SIMS depth profiles of weathered plagioclase and processes affecting dissolved Al and Si in some acidic soils. Nature 334, 336–338.
Nesbitt, H.W., Skinner, W.M., 2001. Early development of Al, Ca, and Na compositional gradients in labradorite leached in pH 2 HCl solutions. Geochimica et Cosmochimica Acta 65, 715–727.
Nesbitt, H.W., Macrae, N.D., Shotyk, W., 1991. Congruent and incongruent dissolution of labradorite in dilute acidic salt solutions. The Journal of Geology 99, 429–442.
Nielsen, A.E., 1986. Mechanisms and rate laws in electrolyte crystal growth from aqueous solution. In: Davis, J.A., Hayes, K.F. (Eds.), Geochemical Processes at Mineral Surfaces. ACS symposium series, vol. 323, pp. 600–614.
Nugent, M.A., Brantley, S.L., Pantano, C.G., Maurice, P.A., 1998. The influence of natural mineral coatings on feldspar weathering. Nature 395, 588–591.
Oelkers, E.H., Schott, J., Devidal, J.-L., 1994. The effect of aluminum, pH, and chemical affinity on the rates of aluminosilicate dissolution reactions. Geochimica et Cosmochimica Acta 58, 2011–2024.
O'Neil, J.R., 1977. Stable isotopes in mineralogy. Physics and Chemistry of Minerals 2, 105–123.
O'Neil, J.R., Taylor Jr., H.P., 1967. The oxygen isotope and cation exchange chemistry of feldspars. American Mineralogist 52, 1414–1437.
Oxburgh, R., Drever, J.I., Sun, Y.-T., 1994. Mechanism of plagioclase dissolution in acid solution at 25 °C. Geochimica et Cosmochimica Acta 58, 661–669.
Penn, R.L., Zhu, C., Xu, H., Veblen, D.R., 2001. Iron oxide coatings on sand grains from the Atlantic coastal plain: high-resolution transmission electron microscopy characterization. Geology 29, 843–846.
Petrovic, R., 1976. Rate control in feldspar dissolution — II: the protective effects of precipitates. Geochimica et Cosmochimica Acta 40, 1509–1522.
Rafal'skiy, R.P., Prisyagina, N.I., Kondrushin, I.B., 1990. Reaction of microcline–perthite with aqueous solutions at 150 and 250 °C. Geochemistry International 27, 56–66.
Schott, J., Brantley, S., Crerar, D., Guy, C., Borcsik, M., Willaime, C., 1989. Dissolution kinetics of strained calcite. Geochimica et Cosmochimica Acta 53, 373–382.

Seyfried Jr., W.E., Janecky, D.R., Berndt, M.E., 1987. Rocking autoclaves for hydrothermal experiments II: the flexible reaction cell system. In: Barnes, H.L., Ulmer, G.C. (Eds.), Hydrothermal Experimental Techniques. Wiley Interscience, pp. 216–240.

Shock, E.L., Helgeson, H.C., 1988. Calculation of the thermodynamic and transport properties of aqueous species at high temperatures and pressures: correlation algorithms for ionic species and equation of state predictions to 5 kb and 1000 °C. Geochimica et Cosmochimica Acta 52, 2009–2036.

Shock, E.L., Sassani, C., Willis, M., Sverjensky, D.A., 1997. Inorganic species in geologic fluids: correlations among standard molal thermodynamic properties of aqueous ions and hydroxide complexes. Geochimica et Cosmochimica Acta 61, 907–950.

Steefel, C.I., van Cappellen, P., 1990. A new approach to modeling water–rock interaction: the role of precursors, nucleation, and Ostwald ripening. Geochimica et Cosmochimica Acta 54, 2657–2677.

Stillings, L.L., Brantley, S.L., 1995. Feldspar dissolution at 25 °C and pH 3: reaction stoichiometry and the effect of cations. Geochimica et Cosmochimica Acta 59, 1483–1496.

Sverjensky, D.A., Shock, E.L., Helgeson, H.C., 1997. Prediction of the thermodynamic properties of aqueous metal complexes to 1000 °C and 5 kb. Geochimica et Cosmochimica Acta 61, 1359–1412.

Tagirov, B., Schott, J., 2001. Aluminum speciation in crustal fluids revisited. Geochimica et Cosmochimica Acta 65, 3965–3992.

Tsuchiya, N., Nakatsuka, K., Yamagishi, Y., 1995. Kinetics and modeling of alkali-feldspar dissolution in a hydrothermal acid solution. In: Khraka, Y.K., Chudaev, O.V. (Eds.), Proceedings of the 8th International Symposium on Water–Rock Interaction. A. A. Balkema, Rotterdam, pp. 161–164.

Wolery, T.J., Daveler, S.A., 1992. EQ6, a Computer Program for Reaction Path Modeling of Aqueous Geochemical Systems: Theoretical Manual, User's Guide, and Related Documentation (version 7.0) UCRL-MA-1 10662 PT IV, Lawrence Livermore National Laboratory, Livermore, CA. 337 pp.

Wollast, R., Chou, L., 1992. Surface reactions during the early stages of weathering of albite. Geochimica et Cosmochimica Acta 56, 3113–3121.

Zhu, C., Blum, A.E., Veblen, D.R., 2004a. Feldspar dissolution rates and clay precipitation in the Navajo aquifer at Black Mesa, Arizona, USA. In: Wanty, R.B., Seal, R.I. (Eds.), Proceedings of the 11th International Symposium on Water–Rock Interaction. A. A. Balkema, New York, pp. 895–899.

Zhu, C., Blum, A.E., Veblen, D.R., 2004b. A new hypothesis for the slow feldspar dissolution in groundwater aquifers. Geochimica et Cosmochimica Acta 68, A148.

Zhu, C., Veblen, D.R., Blum, A.E., Chipera, S.J., 2006. Naturally weathered feldspar surfaces in the Navajo Sandstone aquifer, Black Mesa, Arizona: electron microscopic characterization. Geochimica et Cosmochimica Acta 70, 4600–4616.